

Stress Singularities in Swelling Soft Solids

Alain Goriely*, Johannes Weickenmeier†, and Ellen Kuhl†

*Mathematical Institute, University of Oxford, Oxford UK †Living Matter Laboratory, Stanford University, Stanford USA

When a swelling soft solid is rigidly constrained on all sides except for a circular opening, it will bulge out to expand as observed during decompressive craniectomy, a surgical procedure used to reduce stresses in swollen brains. While the elastic energy of the solid decreases throughout this process, large stresses develop close to the opening. At the point of contact, the stresses exhibit a singularity similar to the ones found in the classic punch indentation problem. Here, we study the stresses generated by swelling and the evolution of the bulging shape associated with this process. We also consider the possibility of damage triggered by zones of either high shear stresses or high fiber stretches.

PACS numbers: 46.25.-y, 87.19.rd

Soft solids play a key role in many biological and physical processes from active gels to swelling polymers [1]. The various patterns that they exhibit under constraints and expansion are known to critically influence both morphogenesis and the design of new micro-devices. A particularly dramatic example of shape formation in swelling soft solids is found in the swelling of the brain. Brain swelling occurs as a consequence of traumatic brain insults such as strokes, tumors, or traumatic brain injury and typically leads to raised intracranial pressure. If the intracranial pressure remains too high, it prevents blood to perfuse properly into the brain tissue and, over time, may cause affected regions of the brain to die by ischemia. Through an osmotic imbalance, this dead tissue induces more swelling that will further propagate damage through the brain [2, 3]. To prevent such a catastrophic cascade, a last recourse consists in performing a *decompressive craniectomy* in which a large portion of the skull is removed to allow the brain to expand. In this highly invasive procedure, the brain mushrooms out of the skull as seen in Fig. 1. If the opening is too small, large stresses develop close to the opening leading to herniation and possible venous occlusion. The bulging may also cause large stretches in axons leading to axonal death and possible long-term disability [4, 5]. It is therefore crucial to understand both the shape and stresses developed in swelling soft solids as a function of the material parameters, swelling, and geometry.

This clinical problem motivates a simple generic physical problem: when a swelling soft solid is constrained to expand except through a circular opening, what is the shape of the bulge? What are the stresses and stretches developed throughout this process? To answer these questions, we first consider a simplified version of the bulging problem where an isotropic elastic solid in frictionless contact with a plate is constrained to swell through a circular opening as seen in Fig. 2. We look for axisymmetric solutions for both the shape and stresses. Finite-element simulations [8] of this problem for different geometries (Fig. 2) reveal the existence of drop-shaped regions of high shear stress close to the contact

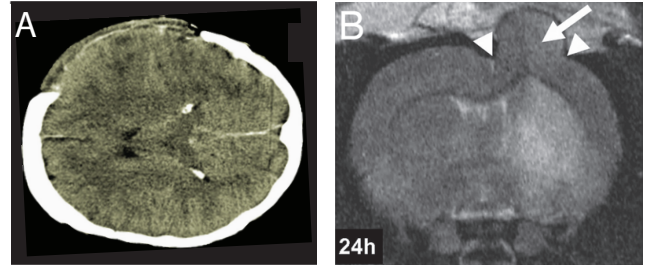


FIG. 1: Brain bulging following decompressive craniectomy. A. Left fronto-temporo-parietal craniectomy in human ([6]). B. MRI showing herniation and resulting ischemia (white arrows) after 24 hours following craniectomy on a rat subject to a middle cerebral artery occlusion [7].

boundary suggesting a singularity in the stresses. These regions, studied experimentally in [9, 10], are reminiscent of the stress localization found in other contact problems such as the Flamant-Cerruti solution [11] for point loading or the punch problem [12–14]. In particular the *bulging problem*, where zero tractions are prescribed on a disk and fixed displacements are given outside the disk, can be seen as the conjugate problem to the cylindrical punch problem where displacements are prescribed over a disk with zero tractions everywhere else. It can also be obtained by taking the proper limit of the annular punch problem [15]. Due to the highly localized nature of this singularity, we expect the same type of stress singularity to appear in various geometries. Bulging due to shear and torsion has also been studied in a classic experiment by Rivlin in connection to Poynting’s effect [16]. This bulging effect has also been used to study the elastic properties of brain tissues [17].

Here, we first consider the exact solution for the bulging problem in linear isotropic elasticity and use it to obtain the bulging shape as well as the stress singularity and the drop regions. We compare and complement this analysis with numerical solutions in large deformations and various geometries, before returning to the brain bulging problem.

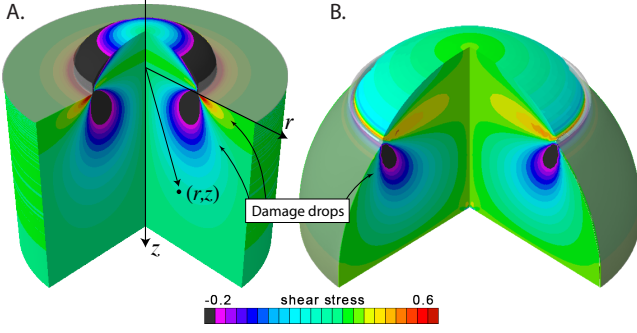


FIG. 2: Bulging simulation. A. Cylindrical geometry. B. Spherical geometry

We first consider an isotropic elastic half-space defined by $\Omega = \{\mathbf{x} = (x, y, z) \in \mathbb{R}^3 | z \geq 0\}$. In this geometry, a deformation is characterized by the displacement of a material point $\mathbf{x} \in \Omega$ to a point $\mathbf{x} + \mathbf{u} \in \mathbb{R}^3$. We use the equivalence between two problems: the first one consists in finding the elastic strains due the uniform swelling of a half-space constrained by a horizontal plane ($z = 0$) with a circular opening. The second one consists in finding the strains developed in a half-space subjected to a fixed vertical displacement (along z) of the boundary everywhere except on a disk. Therefore, uniform swelling in this geometry can be studied within the classical framework of elasticity [18]. Using this equivalence, we assume that the vertical displacements u_z are constant everywhere on the boundary $z = 0$ except in a circular opening of radius one centered at the origin.

In linear elasticity, valid for small displacements, the strain tensor is $\mathbf{E} = \frac{1}{2}(\nabla \mathbf{u} + (\nabla \mathbf{u})^T)$. The Cauchy stress tensor is then $\mathbf{T} = E/(1 + \nu) [\mathbf{E} + \nu/(1 - 2\nu)(\text{tr } \mathbf{E})\mathbf{1}]$ with Young's modulus E , Poisson's ratio ν , and the identity tensor $\mathbf{1}$. In the absence of body forces, the Cauchy equation for elastostatics is $\nabla \cdot \mathbf{T} = \mathbf{0}$. Given the unit normal \mathbf{n} to the boundary, the bulging problem is to determine the displacement and stresses such that $\mathbf{T}\mathbf{n} = \mathbf{0}$ on the unit disk, $u_z = \delta$ outside the unit disk and $\mathbf{T}\mathbf{n} - (\mathbf{n} \cdot \mathbf{T}\mathbf{n})\mathbf{n} = \mathbf{0}$ everywhere on the boundary (i.e. frictionless boundary).

An elegant way to solve this contact problem is to use the Papkovitch-Neuber formulation and introduce a harmonic potential $\phi(r, z)$, in the usual cylindrical coordinates (r, θ, z) , such that

$$\mathbf{u} = \frac{1 + \nu}{E} \left[4(\nu - 1)\boldsymbol{\omega} + \nabla \left(\mathbf{x} \cdot \boldsymbol{\omega} + \frac{\phi}{1 - 2\nu} \right) \right], \quad (1)$$

where $\boldsymbol{\omega} = \mathbf{e}_z \partial \phi / \partial z$. All stresses and displacements can then be obtained from ϕ . For instance, on the surface $z = 0$, we have

$$T_{zz} = -\frac{\partial^2 \phi}{\partial z^2}, \quad u_z = 2\frac{\nu^2 - 1}{E} \frac{\partial \phi}{\partial z}. \quad (2)$$

Therefore, our problem amounts to finding a harmonic

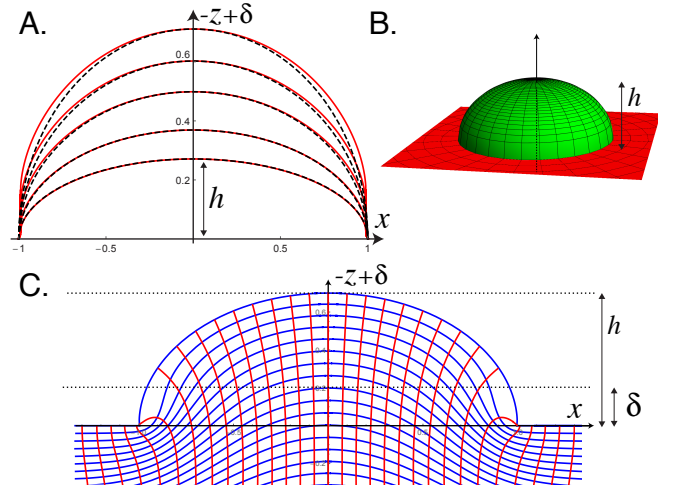


FIG. 3: A. Bulge shapes obtained from the exact linear solution (dashed) compared to the finite-element simulation (solid). B. 3D shape of the bulge (linear solution, $h = 0.733$). C. Internal displacements.

function $\phi = \phi(r, z)$ such that

$$\frac{\partial^2 \phi}{\partial z^2} = 0, \quad 0 \leq r < 1, z = 0, \quad (3)$$

$$\frac{\partial \phi}{\partial z} = \frac{E}{2(\nu^2 - 1)} \delta, \quad r \geq 1, z = 0. \quad (4)$$

Using Collin's method [19, 20], a solution of this problem is found to be

$$\phi = \frac{E\delta}{\pi(\nu^2 - 1)} \Im \left(\int_1^\infty s \mathcal{F}(r, z, s) ds \right), \quad (5)$$

where $\mathcal{F}(r, z, s) = \log \left(\sqrt{r^2 + (z + it)^2} + s + it \right)$. This solution, together with (7), leads to the bulge shape

$$u_z(r) = \delta - h\sqrt{1 - r^2}, \quad r \leq 1, \quad (6)$$

where h is the height of the bulge with volume $V_{\text{bulge}} = 2h\pi/3$. Note that the contact angle is always $\pi/2$ since $u'_z \rightarrow \infty$ as $r \rightarrow 1$. A comparison between this exact solution from linear elasticity and the shape obtained by finite-element simulations is shown in Fig. 3A. Note that, for comparison with the cylindrical geometry, the simulations are done on a finite-size cylindrical domain, taken sufficiently large as to not affect the stress-field close to the opening. For comparison, the parameter h was taken as the maximal value of the simulation at $r = 0$. As expected, for small deformations ($h \lesssim 1/2$), the exact solution provides an excellent description of the profile.

The shear stresses are given by

$$T_{rz} = z \frac{\partial^3 \phi}{\partial \theta \partial z^2}. \quad (7)$$

In Fig. 4, we show that these stresses are in excellent

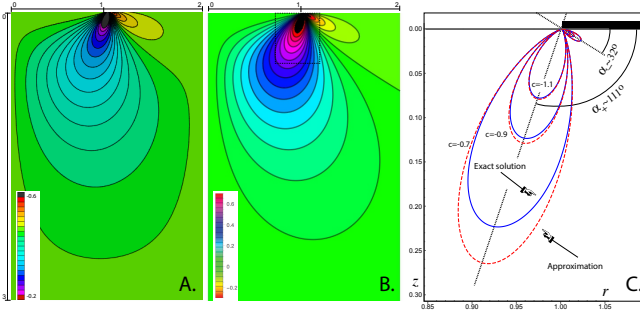


FIG. 4: Shear stress in the reference configuration: A. The numerical simulations and B. the exact solution. C: Comparison between the exact and approximate solution for the damage drops ($c = \epsilon_{\max}/h$, $\nu = 0.45$, $Eh = 1$).

agreement with the ones obtained from finite-element simulations with deviations away from the singularity due to nonlinear and boundary effects. We also observe characteristic *damage drops*, which we defined as regions of high absolute shear stress (regions where $|T_{rz}| > E\epsilon_{\max}/(1+\nu)$ for a fixed maximal shear strain ϵ_{\max}). It is of interest to characterize the volume and orientation of these regions as a function of the size of the bulge h . For large enough ϵ_{\max} , these regions are localized close to the contact boundary. It is therefore possible to simplify the rather cumbersome exact solution by considering its asymptotic expansion for small values of ρ , where ρ is the distance between a material point and the boundary point ($r = 1 + \rho \cos \alpha$, $z = \rho \sin \alpha$). To order $\mathcal{O}(\rho^{3/2})$, we find

$$T_{rz}^{\text{app}} = \frac{E}{4\sqrt{2}(1-\nu^2)} \frac{h}{\sqrt{\rho}} \times \sin \alpha \left(\cos \frac{3\alpha}{2} - \frac{\rho}{4} \left(6 \cos \frac{\alpha}{2} + \cos \frac{5\alpha}{2} \right) \right). \quad (8)$$

The regions such that $|T_{rz}^{\text{app}}| > E\epsilon_{\max}/(1+\nu)$ form two drops as shown in Fig. 4, in reasonable agreement with the exact solution when ϵ_{\max} is large enough. From the dominant terms in (8), the orientations of these two drops is universal and given by

$$\alpha_{\pm} = 2 \cos^{-1} \left(\frac{1}{2} \sqrt{\frac{1}{10} (25 \mp \sqrt{145})} \right). \quad (9)$$

We also recover the expected scaling law $\rho^{-1/2}$ of the stress around the singularity as found in the classic punch problem [14]. The total volume of these drops in the range of validity ($h/\epsilon_{\max} \lesssim 0.5$) is well approximated by $V_{\text{drop}} \approx 0.0183h^2/(\epsilon_{\max}^2(1-\nu^2))$.

Another important quantifier is the stretch of material fibers. Here, we consider the stretch of a material fiber normal to the surface in the reference configuration:

$$\lambda_z = 1 + \frac{1+\nu}{E} \left(z \frac{\partial^3 \phi}{\partial z^3} + (2\nu-1) \frac{\partial^2 \phi}{\partial z^2} \right). \quad (10)$$

As can be seen in Fig. 5, the strain $(\lambda_z - 1)$ reaches a maximal value on the axis of symmetry ($r = 0$). This maximum is located at $z_{\max} = \sqrt{\nu/(2-\nu)}$. At this point, the stretch becomes maximal in the incompressible limit ($\nu \rightarrow 1/2$):

$$\lambda_{\max} = \max_{\nu \in [0, 1/2]} \lambda_z(z_{\max}) = \lambda_z\left(\frac{1}{\sqrt{3}}\right) = 1 + \frac{3\sqrt{3}h}{8}. \quad (11)$$

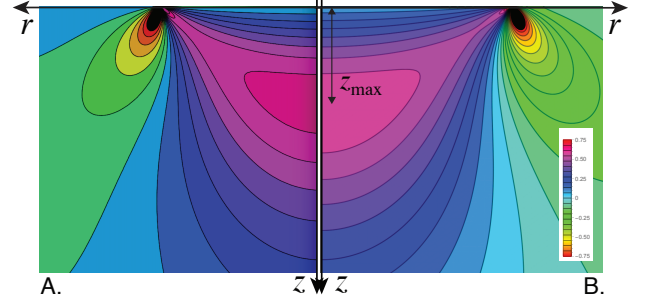


FIG. 5: Vertical strain in the reference configuration. The maximal value of the stretch is reached on the axis of symmetry. A. Finite-element simulation. B. Exact linear solution ($\nu = 0.45$, $Eh = 1$).

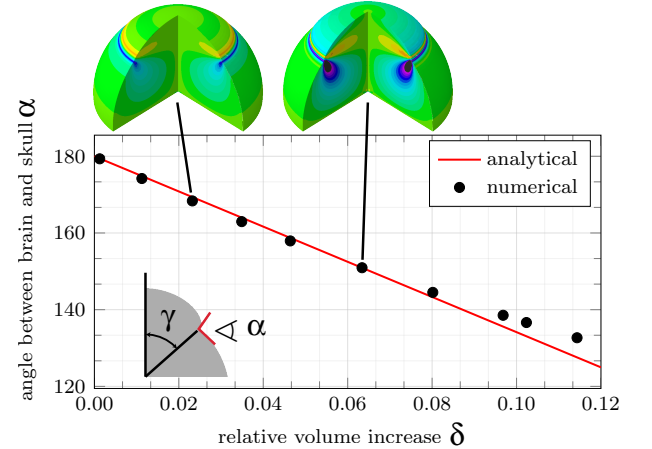


FIG. 6: Swelling in spherical symmetry. The bulging angle as a function of swelling compared to the geometric estimate obtained by overlapping spheres ($\gamma = 50^\circ$).

We now consider bulging in large deformations. For larger swelling, the bulge extends not only radially but also tangentially as shown in Fig. 6. An interesting indicator of the shape is the angle between the tangent to the bulge and the tangent to the sphere as shown in Fig. 6. We compare this angle with a purely geometric estimate obtained by computing the angle between two overlapping spheres as a function of the relative volume increase (i.e. added volume/original volume):

$$\alpha = \pi - 4/3\delta \tan^{-2/3}(\gamma/2)/(1 + \cos \gamma) + \mathcal{O}(\delta^2), \quad (12)$$

where γ is the opening angle. The favorable comparison with the simulation performed in spherical geometry [21] and shown in Fig. 6 indicates that in large deformations the bulge tends to sphere up uniformly. We also note that the damage drops appear in the same regions even for large deformations and no appreciable finite-size effects are found.

We now return to the original brain problem. Clearly, the brain is a much more complex material nonlinear structure with multi-layers and multi-components. Yet, the simple estimates obtained above can provide a useful guide in further studies. In particular, there are two possible well-know types of damage during craniectomy. The first one is herniation due to high stress close to the contact points. These regions of high shear stresses correspond to the damage drops and, due to their universal nature, we expect to observe similar structures in more complex geometries as seen in Fig. 2. The second one is axonal damage due to the stretching of axon. It is known that axonal damage may appear for strains as low as 4% [5]. We conclude that even if we restrict deformations so that all fiber strains remain below 20%, the maximal value of the deformation given by $\lambda_{\max}(h) = 1.2$ is $h \approx 0.3$, a relatively modest size bulge compared to the ones shown in Fig. 1.

In order to check the possible relevance of these results in the actual problem of decompressive craniectomy, we consider the isotropic and homogeneous swelling of an elastic material whose undeformed shape is a brain encased in a skull and compute the stress profile in order to obtain regions where damages may first appear [22]. The material is constrained by the skull except through an opening where it can bulge out. We model the elastic response of the material by a Mooney-Rivlin strain-energy density with independent coefficients for white and grey matters as well as cerebellum and cerebral spinal fluid [23] based on various experimental data sets [24, 25] (See Supplemental Material at [URL will be inserted by publisher] for a description of the code). Swelling is modeled through a multiplicative decomposition of the deformation gradient [26]. The simulation of a decompressive craniectomy shown in Fig. 7 reproduces the characteristic bulging observed clinically. This simulation indicates the existence of very high stresses close to the contact point and elongated regions of high shear stress, reminiscent to the damage drops obtained in simpler geometries, as well as a region of high fiber stretch below the surface as expected from the idealized case.

Initially motivated by the problem of decompressive craniectomy, the analysis of bulging in swelling soft solids reveals a number of interesting features that are found universally: During bulging, the stress develops a singularity that scales as the inverse square root of the distance to the opening. Regions of high shear stresses are characterized by finite regions, i.e. the damage drops, whose orientations close to the singularity, were

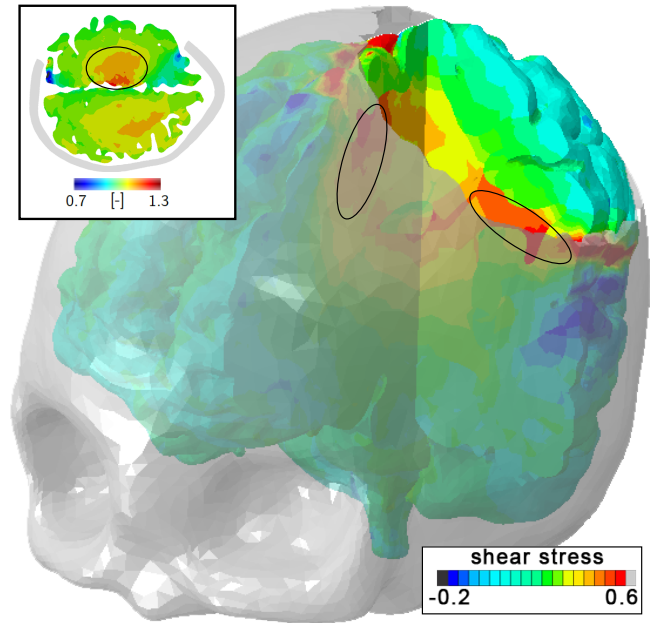


FIG. 7: Finite-element simulation for 10% brain swelling. Regions of high shear stress are circled. Insert: Transverse section showing radial fiber stretch. Region of high radial stretch is circled.

characterized explicitly. Moreover, regions of high vertical strains, representing potential axonal damage, are located around the axis of symmetry and can be quantified by the height of the bulge. We expect these features to be universal in other bulging problems since, close enough to the boundary, stresses and deformations are highly localized.

Acknowledgments This work was supported by the NIH Grant U54GM072970 to Ellen Kuhl. The authors are grateful to Michael Sutcliffe for sharing data and an earlier version of a manuscript and to Michel Destade for discussions on Rivlin's work.

-
- [1] M. Ben Amar, A. Goriely, M. M. Müller, and L. F. Cugliandolo, *New Trends in the Physics and Mechanics of Biological Systems: Ecole de Physique Des Houches; Session XC, 6-31 July 2009* (Oxford University Press, 2011).
 - [2] G. E. Lang, P. S. Stewart, D. Vella, S. L. Waters, and A. Goriely, *J. R. Soc. Interface* **11**, 20140123 (2014).
 - [3] G. E. Lang, D. Vella, S. L. Waters, and A. Goriely, *Biomechanics and Modelling in Mechanobiology* **14**, 1197 (2015).
 - [4] D. J. Cooper, J. V. Rosenfeld, L. Murray, Y. M. Arabi, A. R. Davies, P. D'Urso, T. Kossmann, J. Ponsford, I. Seppelt, P. Reilly, et al., *New England J. Med.* **364**, 1493 (2011).
 - [5] A. Goriely, M. G. D. Geers, G. A. Holzapfel, J. Jayamo-

- han, A. Jérusalem, S. Sivaloganathan, W. Squier, J. A. W. van Dommelen, S. L. Waters, and E. Kuhl, *Biomech. Model. Mechanobiol.* **14**, 931 (2015).
- [6] I. Timofeev and P. J. Hutchinson, *Injury* **37**, 1125 (2006).
- [7] M. Walberer, N. Ritschel, M. Nedelmann, K. Volk, C. Mueller, M. Tschernatsch, E. Stolz, F. Blaes, G. Bachmann, and T. Gerriets, *J. Neurosurg.* **109**, 287 (2008).
- [8] *Abaqus 6.14. Analysis User's Manual*. (SIMULIA. Dassault Systèmes., 2014).
- [9] T. L. Fletcher, A. G. Kolas, P. J. A. Hutchinson, and M. P. F. Sutcliffe, *PloS one* **9**, e102131 (2014).
- [10] T. L. Fletcher, B. Wirthl, A. G. Kolas, H. Adams, P. J. Hutchinson, and M. P. Sutcliffe, *Annals of Biomedical Engineering* pp. 1–15 (2016).
- [11] V. Cerruti, *R. Accad. Lincei Mem. Cl. Sci. Fis. Mat. e Nat.* **3**, 81 (1882).
- [12] N. I. Muskhelishvili, *Some basic problems of the mathematical theory of elasticity* (Springer Science & Business Media, 1977).
- [13] G. M. L. Gladwell, *Contact problems in the classical theory of elasticity* (Springer Science & Business Media, 1980).
- [14] K. L. Johnson, *Contact mechanics* (Cambridge university press, 1987).
- [15] A. B. Roitman and S. F. Shishkanova, *International Applied Mechanics* **9**, 725 (1973).
- [16] R. S. Rivlin, *Journal of Applied Physics* **18**, 444 (1947).
- [17] M. Destrade, M. Gilchrist, J. Murphy, B. Rashid, and G. Saccomandi, *International Journal of Non-Linear Mechanics* **75**, 54 (2015).
- [18] J. Weickenmeier, E. Kuhl, and A. Goriely, *Journal of the Mechanics and Physics of Solids* **DOI information: 10.1016/j.jmps.2016.08.009** (2016).
- [19] W. D. Collins, *Proceedings of the Edinburgh Mathematical Society (Series 2)* **13**, 235 (1963).
- [20] J. R. Barber, *Elasticity* (Springer, 1992).
- [21] J. Weickenmeier, P. Saez, E. Kuhl, and A. Goriely, *Preprint* (2016).
- [22] J. Weickenmeier, C. Butler, P. G. Young, G. A., and E. Kuhl, *Computer Methods in Applied Mechanics and Engineering* (2016).
- [23] A. Goriely, S. Budday, and E. Kuhl, *Advances in Applied Mechanics* **48**, 79 (2015).
- [24] L. A. Mihai, L. Chin, P. A. Janmey, and A. Goriely, *J. R. Soc. Interface* **12**, 20150486 (2015).
- [25] J. Weickenmeier, R. de Rooij, S. Budday, P. Steinmann, T. Ovaert, and E. Kuhl, *Acta Biomaterialia* **42**, 265 (2016).
- [26] D. Ambrosi, G. A. Ateshian, E. M. Arruda, S. C. Cowin, J. Dumais, A. Goriely, G. A. Holzapfel, J. D. Humphrey, R. Kemkemer, E. Kuhl, et al., *J. Mech. Phys. Solids* **59**, 863 (2011).